



α -Substitution effect of fluorine atoms in the cobalt-catalyzed hydrosilylation of fluorine-containing aromatic ketones



Tatsuya Kumon, Siti Asiah Binti Mohd Sari, Shigeyuki Yamada, Tsutomu Konno*

Faculty of Molecular Chemistry and Engineering, Kyoto Institute of Technology, Matsugasaki, Sakyo-ku, Kyoto 606-8585, Japan

ARTICLE INFO

Keyword:

Fluorine
Cobalt catalyst
Hydrosilylation
Fluorinated ketone
Silane

ABSTRACT

Hydrosilylation of fluorine-containing aromatic ketones with triethylsilane in the presence of a catalytic amount of a low-cost and an environmentally benign cobalt catalyst proceeded very smoothly to give the corresponding adducts. Interestingly, this hydrosilylation reaction was not applicable to non-fluorinated ketones. As revealed by density functional theory analysis, a fluorine substituent at the α -position plays a crucial role in facilitating the hydrosilylation reaction.

1. Introduction

Transition metal-catalyzed hydrosilylation reaction of carbon–carbon multiple bonds or a carbonyl group is well recognized as one of the most elegant and reagent economical approaches to prepare organosilicon compounds, which are useful intermediates in the fields of medicinal and materials chemistry [1]. Owing to the broad utility of the hydrosilylation reaction, extensive studies on the development of efficient hydrosilylation protocols using transition metal catalysts have been conducted so far, and many useful hydrosilylative transformations using catalysts based on late transition metals such as Pt, Pd, Rh, Ru, and Ir have been reported [2–5]. However, owing to the environmental impact and resource depletion associated with the use of precious-metal catalysts, the development of alternative hydrosilylation protocols using environmentally friendly and inexpensive transition metal catalysts is necessary. Consequently, significant research effort has been devoted to the development of hydrosilylation reactions using catalysts based on first-row transition metals such as Fe [6], Co [7], and Cu [8], which are naturally abundant, economical, and less toxic. The broad utility of such catalysts for hydrosilylation reactions has been demonstrated over the past decade [6–8].

Our research group has hitherto devoted extensive effort to the development of fluorinated functional materials [9], fluorinated synthetic intermediates [10], and transition metal-catalyzed synthetic transformations [11] in order to establish useful synthetic protocols for a wide variety of organofluorine compounds. Notably, in the course of a recent research project on transition metal-catalyzed transformations, our interest was directed toward the development of novel synthetic protocols for organofluorine compounds using first-row transition

metal catalysts. We have reported that the $\text{Co}_2(\text{CO})_8$ -catalyzed hydrosilylation of fluoroalkylated internal alkynes [12a] or β -fluoroalkyl- α,β -unsaturated ketones [12b] proceed successfully to afford the corresponding fluorine-containing vinyl silanes or 1,4-hydrosilylated enol silane derivatives, respectively, demonstrating the potent utility of low-cost and environmentally benign cobalt catalysts for the effective synthesis of organofluorine compounds (Fig. 1A).

During our extensive investigation, fluorine-containing ketones were effectively transformed into the corresponding silyl-protected fluorinated alcohols by cobalt-catalyzed hydrosilylation (Fig. 1B) [13]. In addition, it was observed that the catalyst system is not applicable to non-fluorinated ketones, i.e., fluorine atoms in the substrate are crucial for the cobalt-catalyzed hydrosilylation process. In this article, we discuss the cobalt-catalyzed hydrosilylation of fluorine-containing ketones in detail. Furthermore, a reaction mechanism that rationalizes the unique α -substitution effect exerted by a fluorine atom is proposed based on the results of density functional theory (DFT) calculations.

2. Results and discussion

2.1. Screening of reaction conditions

An initial screening of the reaction conditions for cobalt-catalyzed hydrosilylation reactions was undertaken using the α,α,α -trifluoroacetophenone derivative **1aA**. The results are summarized in Table 1.

Upon refluxing **1aA** with Et_3SiH (1.2 equiv.) in dichloroethane in the presence of a catalytic amount of $\text{Co}_2(\text{CO})_8$ (5.0 mol%) for 3 h, the desired hydrosilylation occurred smoothly to afford the corresponding

* Corresponding author.

E-mail address: konno@kit.ac.jp (T. Konno).

(A) Previous works: Cobalt-catalyzed hydrosilylation of alkynes or fluorinated enones

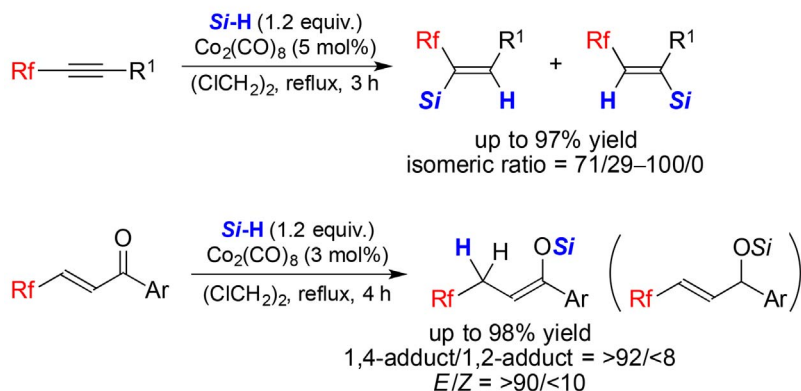


Fig. 1. Cobalt-catalyzed transformations of fluorine-containing molecules.

(B) This work: Cobalt-catalyzed hydrosilylation of fluorinated ketones

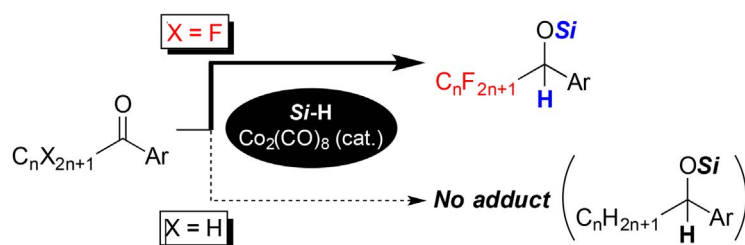


Table 1
Initial screening of hydrosilylation conditions.

Entry	Solvent	Si-H	X/mol%	Yield ^a /% of 2aA	Recovery ^a /% of 1aA
1	ClCH ₂ CH ₂ Cl	Et ₃ SiH	5.0	75	18
2	Hexane	Et ₃ SiH	5.0	Quant.	00
3	Toluene	Et ₃ SiH	5.0	Quant.	00
4	Toluene	Et ₃ SiH	3.0	Quant.	00
5	Toluene	Et ₃ SiH	1.0	Quant. (84)	00
6	Toluene	Et ₃ SiH	0.5	80	18
7	Toluene	Et ₃ SiH	0.0	Trace	90
8	Toluene	PhMe ₂ SiH	1.0	23	73
9	Toluene	(EtO) ₃ SiH	1.0	76	10
10	Toluene	Me(EtO) ₂ SiH	1.0	69	18
11	Toluene	<i>i</i> -Pr ₃ SiH	1.0	00	Quant.

^a Determined by ¹⁹F NMR. Value in parentheses is the isolated yield.

adduct **2aA** in 75% yield (Table 1, entry 1). As shown in Table 1, entries 2 and 3, replacing the solvent with hexane or toluene provided significant improvement in the yield, leading to quantitative formation of **2aA**. With a lower catalyst loading (1.0–3.0 mol%), the hydrosilylated adduct **2aA** is obtained in a quantitative yield as well (entries 4 and 5). However, further decrease in catalyst loading (0.5 mol%) resulted in the sluggish formation of the hydrosilylation product (entry 6). Furthermore, no **2aA** was obtained in the absence of the Co₂(CO)₈ catalyst (entry 7). Thus, the presence of the cobalt catalyst was crucial for the hydrosilylation of fluorinated ketone **1aA**. Other reductants instead of Et₃SiH, including PhMe₂SiH, (EtO)₃SiH, and Me(EtO)₂SiH, also participated in the cobalt-catalyzed hydrosilylation reaction, although the yields of **2aA** were slightly lower (entries 8–10). In sharp contrast, the use of *i*-Pr₃SiH as a reductant was not suitable for the present cobalt-

catalyzed hydrosilylation protocol, resulting in quantitative recovery of **1aA**. These results indicate that hydrosilanes possessing bulky substituents tend to suppress the formation of the desired hydrosilylation adduct. Informed by these experiments, we selected the reaction conditions shown in Table 1, entry 5 as optimal for the present cobalt-catalyzed hydrosilylation.

2.2. Substrate scope of the cobalt-catalyzed hydrosilylation reaction

Using the optimal reaction conditions, we performed cobalt-catalyzed hydrosilylation reactions using various fluorinated ketones (**1a**). The results obtained are presented in Table 2.

Hydrosilylation of α,α,α -trifluoroacetophenone (**1aB**), which has no substituents on the aromatic ring, with 1.2 equiv. of Et₃SiH in the

Table 2
Cobalt-catalyzed hydrosilylation of different fluorinated ketones.

Entry	R	Product	Yield ^a / % of 2a	Recovery ^{a,b} / % of 1a
01	4-MeC ₆ H ₄ (A)	2aA	Quant. (84)	00
02	Ph (B)	2aB	71	18
03 ^c	Ph (B)	2aB	Quant. (83)	00
04	4-MeOC ₆ H ₄ (C)	2aC	Quant. (95)	00
05	3-MeOC ₆ H ₄ (D)	2aD	Quant. (84)	Trace
06	2-MeOC ₆ H ₄ (E)	2aE	24	66
07 ^c	2-MeOC ₆ H ₄ (E)	2aE	91 (80)	09
08	4-FC ₆ H ₄ (F)	2aF	19	39
09	4-ClC ₆ H ₄ (G)	2aG	19	81
10 ^d	4-ClC ₆ H ₄ (G)	2aG	94 (89)	Trace
11	1-Naphthyl (H)	2aH	47	46
12 ^e	1-Naphthyl (H)	2aH	96 (95)	00
13	<i>n</i> -C ₁₀ H ₂₁ (I)	2aI	Trace	95
14 ^e	<i>n</i> -C ₁₀ H ₂₁ (I)	2aI	Trace	93

^a Determined by ¹⁹F NMR. Values in parentheses are the isolated yields.

^b Indicated combined yield of 1a and the corresponding hydrate.

^c Carried out for 18 h.

^d With 5.0 mol% of Co₂(CO)₈ and 1.5 equiv. of Et₃SiH.

^e With 3.0 mol% of Co₂(CO)₈ and 1.5 equiv. of Et₃SiH.

presence of 1.0 mol% Co₂(CO)₈ in toluene at reflux temperature for 3 h proceeded smoothly to afford the corresponding hydrosilylated adduct **2aB** in 71% yield along with a small amount of unreacted **1aB** (entry 2). However, extending the reaction time from 3 to 18 h allowed complete consumption of **1aB**, resulting in the formation of **2aB** in 83% isolated yield (Table 2, entry 3). Reaction of **1aC** or **1aD** with a strong electron-donating group, i.e. a methoxy group, on the benzene ring at the *para* or *meta* position, respectively, proceeded very well to afford the corresponding silyl ether **2aC** or **2aD** in 95% or 84% yield, respectively (entries 4 and 5). In sharp contrast, the reaction of fluorinated ketone **1aE** with a methoxy group at the *ortho* position under the same conditions became sluggish, leading to the formation of **2aE** in only 24% NMR yield and 66% recovery of **1aE** as a mixture of the hydrate forms (entry 6). After several attempts, it was found that extending the reaction time to 18 h led to the formation of **2aE** in high isolated yield (entry 7). Conversely, fluorinated ketones **1aF** and **1aG** having an electron-withdrawing fluoro or chloro substituent, respectively, on the benzene ring at the *para* position were observed to be less reactive for the present hydrosilylation reaction, with the corresponding **2aF** and

2aG both being obtained in only 19% yield, respectively (entries 8 and 9). In these cases, the unreacted starting substrates **1aF** and **1aG** were obtained in 39% and 81% recovery yields, respectively, as mixtures of the hydrate forms. The distinct difference in the recovery yields of **1aF** and **1aG** may be caused by their thermal properties, including boiling point and volatility. **1aF** had a lower boiling point (66–67 °C/34 Torr [14a]), which was close to the reflux temperature of toluene (110.6 °C/760 Torr), than that of **1aG** (183 °C/760 Torr [14b]). However, upon treating **1aG** with increased amounts of Et₃SiH (1.5 equiv.) and Co₂(CO)₈ (5.0 mol%) in toluene at reflux for 3 h, the hydrosilylation proceeded very smoothly to afford **2aG** in 94% NMR (89% isolated) yield. Although the hydrosilylation of the sterically bulky 1-naphthyl trifluoromethyl ketone (**1aH**) under the optimal conditions was somewhat sluggish (Table 2, entry 11), a dramatic improvement in the yield of **2aH** (95% isolated yield) became observed when the reaction was carried out using 1.5 equiv. of Et₃SiH and 3.0 mol% Co₂(CO)₈ (entry 12). As shown in entries 13 and 14, the use of the aliphatic fluorinated ketone **1aI** was not applicable to the present cobalt-catalyzed hydrosilylation protocol and results in a large recovery of **1aI** (> 93%) as a mixture with the hydrate forms, despite extensive attempts to identify suitable reaction conditions.

Subsequently, we examined the cobalt-catalyzed hydrosilylation reaction using different aromatic ketones with a variety of fluoroalkenyl moieties (**1b–e**). The results obtained are summarized in Table 3.

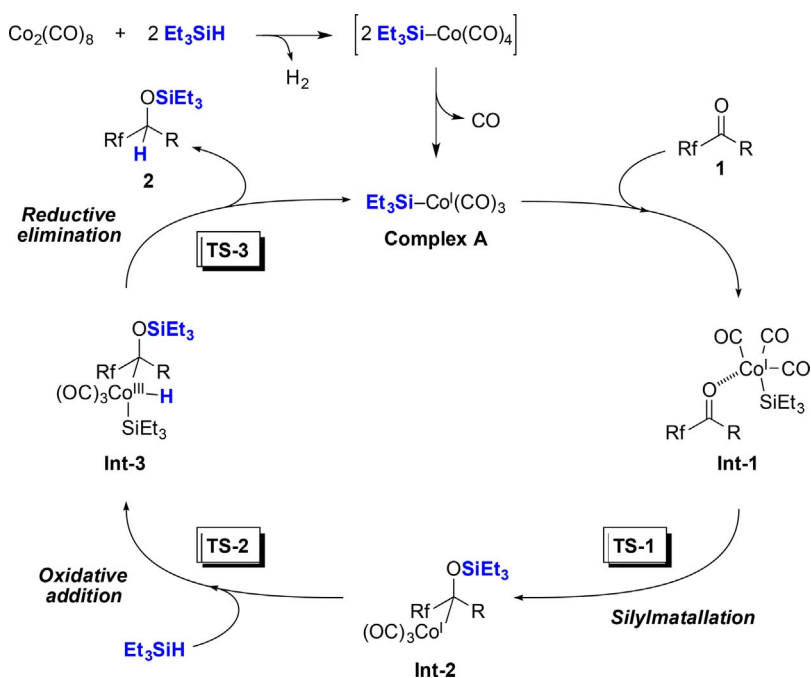
Using the optimal reaction conditions presented in entry 5 in Table 1, reaction of the fluorinated aromatic ketone **1bA** carrying a *n*-C₃F₇ moiety with 1.2 equiv. of Et₃SiH in the presence of 1.0 mol% Co₂(CO)₈ in toluene at reflux for 3 h did not provide satisfactory results, leading instead to a large recovery of **1bA** (entry 2). Upon further investigation, the reaction efficiency using **1bA** was significantly improved, with the corresponding hydrosilylated adduct **2bA** being obtained in 93% isolated yield when the reaction was conducted with 1.5 equiv. of Et₃SiH in the presence of 6.0 mol% Co₂(CO)₈ for 24 h (entry 3). As can be seen in entries 4–5, the use of 2,3,4,5,6-pentafluorobenzophenone (**1cB**), where Rf = C₆F₅ and R = Ph, as a substrate was not applicable to the present cobalt-catalyzed hydrosilylation protocol, despite several attempts to identify suitable reaction conditions. This drastic suppression of the hydrosilylation process is most likely caused by a combination of the steric bulkiness and low solubility of **1cB** in toluene. When the α,α-difluoroacetophenone derivative **1dA** was used in the present protocol, the reaction proceeded very well to give rise to the corresponding adduct **2dA** in quantitative (97% isolated) yield (entry 6). In contrast, the use of the α-fluoroacetophenone derivative **1eA** as a substrate drastically retarded the reaction and a large amount (83%) of unreacted **1eA** and its hydrate were recovered

Table 3
Cobalt-catalyzed hydrosilylation using different aromatic ketones.

Entry	Rf	R	Product	Yield ^a / % of 2	Recovery ^{a,b} / % of 1
01	CF ₃ (a)	4-MeC ₆ H ₄ (A)	2aA	Quant. (84)	00
02	<i>n</i> -C ₃ F ₇ (b)	4-MeC ₆ H ₄ (A)	2bA	6	94
03 ^b	<i>n</i> -C ₃ F ₇ (b)	4-MeC ₆ H ₄ (A)	2bA	Quant. (93)	00
04	C ₆ F ₅ (c)	Ph (B)	2cB	0	99
05 ^b	C ₆ F ₅ (c)	Ph (B)	2cB	20	73
06	CF ₂ H (d)	4-MeC ₆ H ₄ (A)	2dA	Quant. (97)	0
07	CFH ₂ (e)	4-MeC ₆ H ₄ (A)	2eA	Trace	83
08	CH ₃ (f)	4-MeC ₆ H ₄ (A)	2fA	0	(94)
09	CO ₂ Et (g)	Ph (B)	2gB	0	(89)

^a Determined by ¹⁹F NMR. Values in parentheses are the isolated yields.

^b Carried out for 24 h using 6.0 mol% of Co₂(CO)₈ and 1.5 equiv. of Et₃SiH.



Scheme 1. Possible reaction mechanism for cobalt-catalyzed hydrosilylation.

(entry 7). These results imply that the number of fluorine atoms at the α -position is an important factor for the cobalt-catalyzed hydrosilylation reaction.

In order to clarify the effect of the fluorine substituent at the α -position in the present hydrosilylation protocol, we also examined cobalt-catalyzed hydrosilylation reaction using ketones and aldehydes without any fluorine substituents such as **1fA** and **1gB**, and the results are also listed in Table 3. As shown in Table 3, entry 8, the reaction using the non-fluorinated acetophenone derivative **1fA** did not proceed at all, resulting in almost quantitative recovery (94%) of unreacted **1fA**. When ethyl phenylglyoxylate (**1gB**), where $\text{Rf} = \text{CO}_2\text{Et}$ and $\text{R} = \text{Ph}$ and in which the CO_2Et group had a similar electron-withdrawing nature to that of the CF_3 moiety in **1aA** [15], was adopted as the substrate, no reaction occurred. These results indicate that the cobalt-catalyzed hydrosilylation is far more influenced by the steric bulkiness around the carbonyl moiety than its electronic nature.

2.3. Possible reaction mechanism

A possible reaction mechanism for the cobalt-catalyzed hydrosilylation of fluorinated ketones is shown in Scheme 1 [16,17].

The reaction of $\text{Co}_2(\text{CO})_8$ with two equivalents of Et_3SiH generates the silylcobalt precatalyst $\text{Et}_3\text{Si-Co}(\text{CO})_4$ accompanied by hydrogen gas evolution. This precatalyst immediately eliminates CO to generate the active silylcobalt complex $\text{Et}_3\text{Si-Co}(\text{CO})_3$ (Complex A) [16]. The active Complex A has a vacant d orbital on the cobalt atom and undergoes coordination by the carbonyl oxygen of **1** to form Int-1, which is subjected to silylmatalation to form Int-2 via a transition state (TS-1). Subsequent oxidative addition of the $\text{Co}(\text{I})$ species in Int-2 to the Si-H bond of unreacted Et_3SiH furnishes $\text{Co}(\text{III})$ -intermediate (Int-3) via TS-2, which immediately undergoes reductive elimination via TS-3 to afford the desired hydrosilylated adduct **2** along with regeneration of the active $\text{Et}_3\text{Si-Co}(\text{CO})_3$ complex. The detailed reaction mechanism using a quantum chemical calculation will be discussed in Section 2.4.

In order to figure out the actual composition of the cobalt catalyst, we demonstrated the hydrosilylation reaction of α,α,α -trifluoroacetophenone (**1aB**) using pre-generated $\text{Et}_3\text{Si-Co}(\text{CO})_4$ prepared in advance as a catalyst (Scheme 2).

The silylcobalt complex was prepared according to a previous literature method [16]. Upon treating $\text{Co}_2(\text{CO})_8$ with 3.0 equiv. of Et_3SiH

at room temperature for 0.5 h followed by removal of the excess Et_3SiH , $\text{Et}_3\text{Si-Co}(\text{CO})_4$ was successfully obtained as a brown oil. The structure was confirmed by typical spectroscopic measurements such as NMR and IR. IR analysis confirmed the disappearance of the Si-H stretching vibration (2100 cm^{-1}) of Et_3SiH and the signal associated with the bridging $\text{C}=\text{O}$ bond (1860 cm^{-1}) of $\text{Co}_2(\text{CO})_8$. With the pre-generated $\text{Et}_3\text{Si-Co}(\text{CO})_4$ in hand, we performed a cobalt-catalyzed hydrosilylation reaction using **1aB** in toluene at reflux temperature for 3 h and successfully obtained the corresponding product **2aB** in 91% isolated yield. Thus, it was safely concluded that the actual pre-catalyst was $\text{Et}_3\text{Si-Co}(\text{CO})_4$.

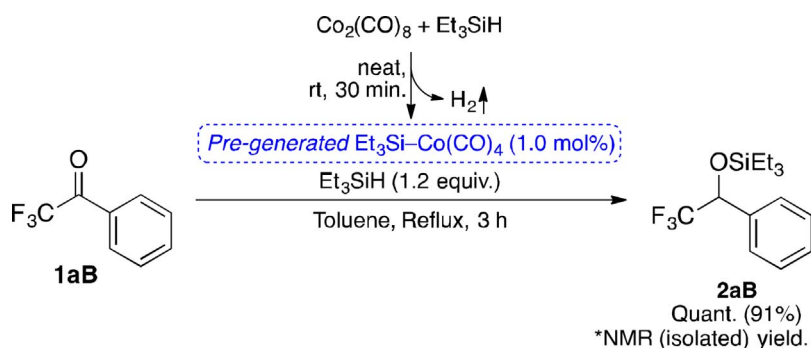
To gain further information on the reaction mechanism, a crossover experiment for the hydrosilylation reaction was carried out using an equimolar amount of α,α,α -trifluoroacetophenone (**1aB**) and the non-fluorinated acetophenone **1fB** under the optimal conditions shown in Table 1, entry 5 (Scheme 3).

The treatment of a mixture of **1aB** and **1fB** (1.0 equiv. each) with 1.2 equiv. of Et_3SiH in the presence of 1.0 mol% $\text{Co}_2(\text{CO})_8$ in toluene at reflux temperature for 3 h unexpectedly afforded neither **2aB** nor **2fB**, resulting instead in the quantitative recovery of both **1aB** and **1fB**.

2.4. Theoretical evaluation of the reaction mechanism

2.4.1. Effect of fluorine-substitution at the α -position

In order to gain more information on the reaction mechanism, we carried out a theoretical study using a Gaussian 09W with a density functional theory (DFT) at the B3LYP/6-31 + G(d,p) level of theory as a basis set [18]. To explore the pathway of the cobalt-catalyzed hydrosilylation reaction using fluorinated ketone **A** as well as the non-fluorinated ketone **B** by DFT calculation, $\text{Me}_3\text{Si-Co}(\text{CO})_3$ was adopted as a model catalyst structure and Me_3SiH as a reductant. The DFT calculation elucidated the presence of three transition states, i.e., those for the silylmatalation step (TS-1), the oxidative addition step (TS-2), and the reductive elimination step (TS-3), and the geometry of the transition states was characterized by vibrational analysis, which confirmed that the obtained geometries possess a single imaginary frequency. Reaction pathways were traced by the intrinsic reaction coordinate (IRC) method [19] to obtain the energy-minimum geometries, and IRC analysis of TS-1 provided two energy-minimum geometries, assigned as Int-1 for the reactant and Int-2 for the product. Similarly,



Scheme 2. Cobalt-catalyzed hydrosilylation of **1aB** using pre-generated $\text{Et}_3\text{Si-Co}(\text{CO})_4$ as a catalyst.

IRC analysis of **TS-2** also provided two energy-minimum geometries (**Int-3** for the reactant and **Int-4** for the product). On the basis of the calculation results, energy profiles of the reaction pathways are illustrated in Fig. 2.

The energy profiles revealed that the energy-minimum geometry for fluorinated ketone (**Int-1A**) was $4.5 \text{ kcal mol}^{-1}$ higher than that for the non-fluorinated ketone (**Int-1B**). Thus, the stabilities of **Int-1** were in the order **Int-1A** < **Int-1B**, whereas the stabilities for **TS-1** presented the opposite trend, i.e., **TS-1A** > **TS-1B**. To understand the crossing stability of **Int-1** and **TS-1** between fluorinated ketone **A** and non-fluorinated ketone **B**, the geometries for **Int-1**, **TS-1**, and **Int-2** for **A** and **B** were evaluated in detail. The geometries calculated are shown in Fig. 3 and the observed structural data are summarized in Table 4.

Upon careful observation of the energy-minimum geometries for **Int-1A** and **Int-1B** shown in Table 4, large differences were observed for the Co–O bond lengths, the coordination bond angles $\angle \text{C}^1\text{–O–Co}$, and the dihedral angle (ϕ) between $\text{C}^2\text{–C}^1\text{–O–Co}$, as follows:

- (1) The interatomic distance of Co–O in **Int-1A** was 216 pm, which was 4 pm longer than the coordination bond length in **Int-1B**. The longer Co–O bond length in **Int-1A** may be brought about by the electron-withdrawing character of a CF_3 group, which strongly weakens the Lewis basicity of the carbonyl oxygen.
- (2) The coordination bond angle, $\angle \text{C}^1\text{–O–Co}$, was 153.8° for **Int-1A**, in which the Co atom was existed at the opposite side to the CF_3 moiety. In contrast, the angle for **Int-1B** was 136.2° , and the Co atom was presented at the same side as the CH_3 group (Fig. 3a and d). The steric bulkiness of the substituents were in the order: $\text{Ph} > \text{CF}_3 > \text{CH}_3$ [20], indicating that both **Int-1A** and **Int-1B** should undergo coordination from the same side as the CF_3 or CH_3 moiety. The opposite observation for **Int-1A** indicates that not only steric bulkiness but also the electron-abundance of the CF_3 moiety strongly affect the coordination process to form **Int-1A**. In addition, the bond angle for **Int-1A** deviated more from the ideal angle of the sp^2 hybridized orbital for oxygen (120°) than that for **Int-1B**, which may be due to steric repulsion between the silylcobalt complex and

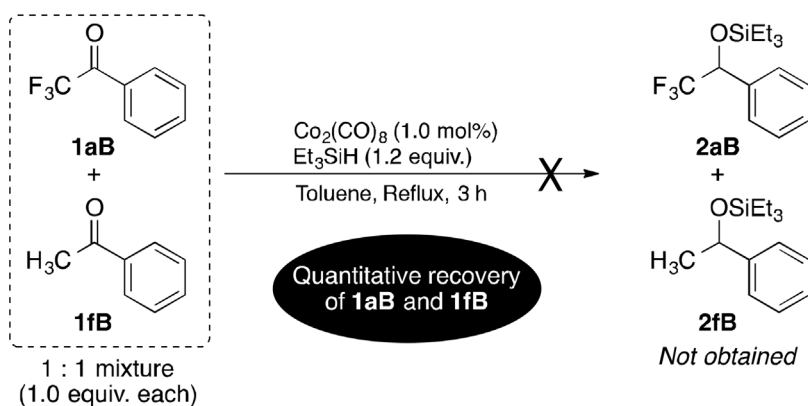
the sterically bulky phenyl group in **Int-1A**.

- (3) The dihedral angle ϕ ($\text{C}^2\text{–C}^1\text{–O–Co}$) in **Int-1A** was 18.3° , which deviated significantly from the plane structure of an ideal carbonyl moiety ($\phi = 0^\circ$), whereas a virtually planar structure ($\phi = 6.6^\circ$) was observed in the case of **Int-1B**.

Taking the above factors into account, it can be concluded that larger deviations from the ideal values for bond length, angle, and dihedral angle in the case of **Int-1A** cause an increase in its total energy and thus a decrease in its relative stability.

Fig. 3 also provided us several understandings on the transition state, **TS-1**, for the silylmetallation process. Thus, analyzing a bond-length of Co–Si for **Int-1** and **TS-1**, dramatically elongated interatomic distance (18 pm each) between $\text{Co}\cdots\text{Si}$ in the **TS-1** was observed in both fluorinated **A** and non-fluorinated **B**; the significant elongation of $\text{Co}\cdots\text{Si}$ bond demonstrates to be completed its bond-breaking during silylmetallation process across the **TS-1**. On the other hand, comparing interatomic distance between $\text{Co}\cdots\text{C}^1$ for both **TS-1** and **Int-2**, a little (only 4–9 pm) change of the interatomic distance was observed in spite of the presence or absence of fluorine-substituents. The similar Co– C^1 bond length between **TS-1** and **Int-2** indicates that bond formation between Co and C^1 atoms is almost completely achieved during the silylmetallation process. Judging from these theoretical insights, the **TS-1** for silylmetallation process could be safely posited as a late-transition state, which generally possesses product-like character and stability; accordingly, it is reasonably concluded that total energy of **TS-1A** for fluorinated ketone is lower than that of **TS-1B** for non-fluorinated one due to the stabilization effect reflected in the stability of **Int-2**. The energetic difference between a transition state and a substance, **TS-1** and **Int-1** in this case, indicates the activation energy (E_a), which can be defined as the minimum energy required for a chemical reaction to occur. The E_a values at each transition state are summarized in Table 5.

Comparing the activation energies for fluorinated **A** and non-fluorinated **B** to across **TS-2** and **TS-3**, there was no difference in the E_a values ($E_a\text{-2A}$, $E_a\text{-2B}$ for **TS-2** and $E_a\text{-3A}$, $E_a\text{-3B}$ for **TS-3**), whereas a significant difference was observed in $E_a\text{-1A}$ and $E_a\text{-1B}$ to cross **TS-1A** or **TS-1B**,



Scheme 3. Crossover experiment for the hydrosilylation reaction using a 1:1 ratio of **1aB** and **1fB** as substrates.

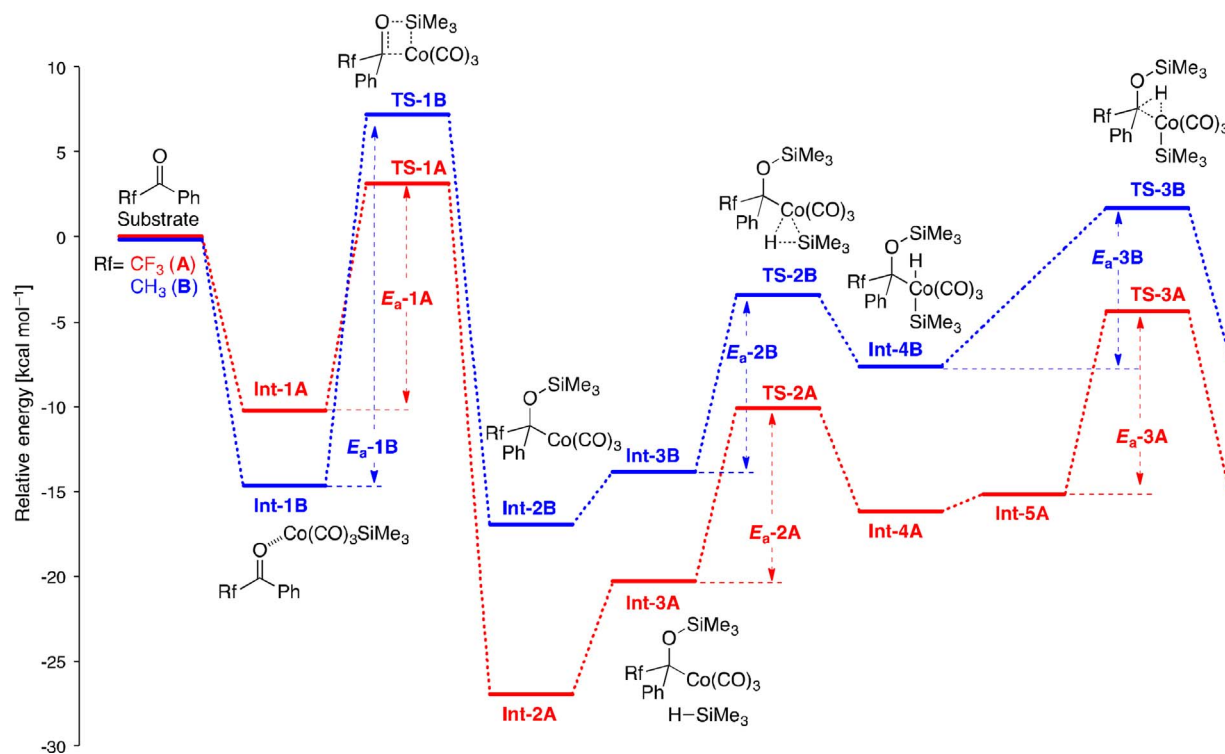


Fig. 2. Energy profiles for the hydrosilylation of fluorinated and non-fluorinated ketones calculated by IRC analysis.

respectively, with E_a -1A being much lower than E_a -1B. This means that the fluorinated ketone can cross TS-1A to form the more stable Int-2A more easily than non-fluorinated substrate can cross TS-1B.

Considering all the theoretical arguments above, it can be assumed that the silylmetalation process is the key reaction step in the cobalt-catalyzed hydrosilylation reaction for the fluorinated ketone, which is attributable to the low value of E_a and the formation of the thermally stable Int-2. In sharp contrast, the non-fluorinated ketone forms a coordination complex (Int-1B) that is more stable than Int-1A, which causes a significant increase in the activation energy E_a required to

cross TS-1B and thus a drastic suppression of further silylmetalation. Taking the results of the crossover experiment shown in Scheme 3 into consideration, the hypothesis is concluded to be reasonable.

2.4.2. Effect of the number of fluorine atoms at the α -position

As mentioned above, our investigation of the present cobalt-catalyzed hydrosilylation revealed an interesting phenomenon in that the CF_3 - and CF_2H -substituted ketones **1aA** and **1dA** are very smoothly converted to the corresponding product, but no adduct was obtained in the case of the CFH_2 -substituted ketone **1eA**. To make this intriguing

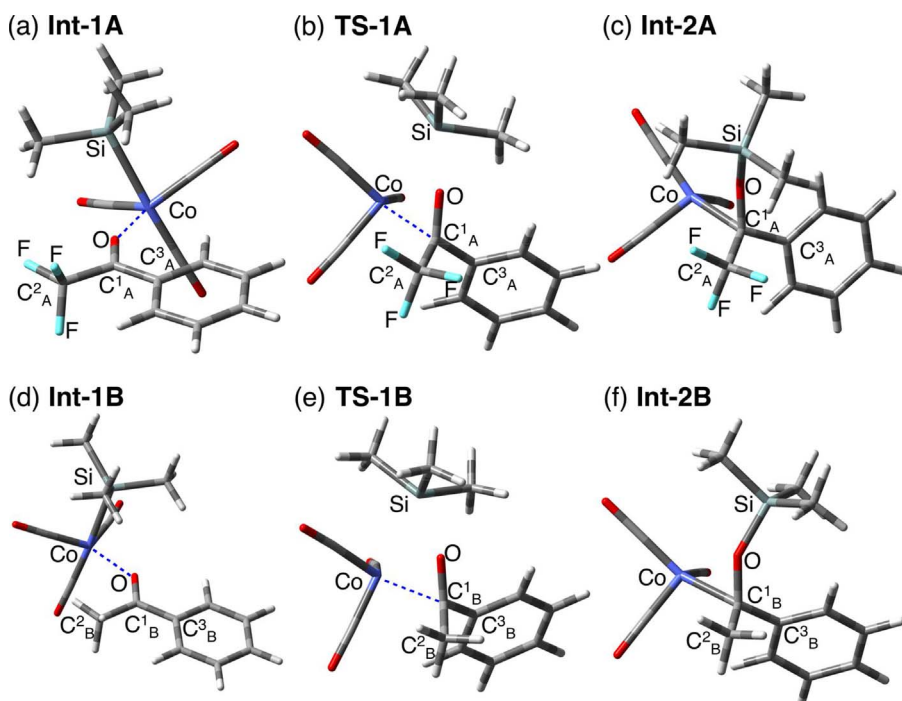


Fig. 3. (a, d) Energy-minimum geometries (Int-1A for the fluorinated ketone and Int-1B for the non-fluorinated ketone) calculated by IRC analysis, (b, e) geometries for TS-1A and TS-1B, and (c, f) energy-minimum geometries for Int-2A and Int-2B calculated by IRC analysis.

Table 4
Structural data for **Int-1**, **TS-1**, and **Int-2** for **A** and **B** calculated by DFT calculations.

	For fluorinated ketone A			For non-fluorinated ketone B		
	Int-1A	TS-1A	Int-2A	Int-1B	TS-1B	Int-2B
$\angle C^1-O-Co$ [°]	153.8	–	–	136.2	–	–
ϕ (C^2-C^1-O-Co) [°]	18.3	–	–	6.6	–	–
Co...O [pm]	216	–	–	212	–	–
Co...Si [pm]	242	260	–	241	259	–
Co...C ¹ [pm]	–	202	198	–	207	198
$\angle C^2-C^1-O$ [°]	115.3	111.1	112.9	120.9	113.6	109.3
$\angle C^2-C^1-C^3$ [°]	119.1	113.1	113.2	120.2	114.3	111.6
$\angle C^3-C^1-O$ [°]	125.5	120.9	114.0	118.9	120.3	118.6

Table 5
Activation energies for each transition state for the fluorinated and non-fluorinated ketones.

	Activation energy [kcal mol ⁻¹]		
	Fluorinated ketone (A)	E_{a-1A} (13.38)	E_{a-2A} (10.21)
Non-fluorinated ketone (B)	E_{a-1B} (21.90)	E_{a-2B} (10.36)	E_{a-3B} (9.28)

phenomenon clear, we carried out further reaction pathway analysis for the cobalt-catalyzed hydrosilylation of CF₂H-substituted (**C**) and CFH₂-substituted (**D**) ketones by DFT calculation with the same theory level and basis set. The energy profiles calculated are shown in Fig. 4, in which only the energy profile for the initial silylmatalation process is shown as it is the key reaction step in the hydrosilylation reaction.

As shown in Fig. 4, DFT calculations revealed the presence of two coordination intermediates (**Int-1C**) for the CF₂H-containing substrate (**C**) and three coordination intermediates (**Int-1D**) for the CFH₂-containing substrate (**D**) in the silylmatalation process. Among the five intermediates, as shown in Fig. 5 and Table 6, the two intermediates **Int-1C**₁ and **Int-1C**₂ possessed larger coordination bond angles of $\angle C^1-O-Co$ and dihedral angles (ϕ) between C²-C¹-O-Co than those of the other three intermediates **Int-1D**, and **Int-1C**₁ exhibited the

largest values ($\angle C^1-O-Co = 151.1^\circ$ and $\phi = 9.95^\circ$), which was due to the effects of both steric hindrance and electron-withdrawal induced by multiple fluorine atoms at the α -position. The large bond angle and dihedral angle in **Int-1C**₁ presented the largest deviations from an ideal sp²-hybridized structural conformation of the five intermediates, which led to higher total energies for **Int-1C** (with the CF₂H-substituent) than those for **Int-1D** (with the CFH₂-substituent).

The fact that the calculated structures at **TS-1** are conformationally similar to that of the intermediate **Int-2** for both the CF₂H- and CFH₂-derivatives clearly demonstrates that the silylmatalation process for these analogues also proceeds via a late transition state [21]. Accordingly, it is clear that the energy level of **TS-1C** for the CF₂H-substituted derivative is lower than that of **TS-1D** for the CFH₂-substituted analogue. The activation energies E_{a-1C} and E_{a-1D} required to cross **TS-1C** and **TS-1D**, respectively, were 13.63 for E_{a-1C} and 16.45 kcal mol⁻¹ for E_{a-1D} . The lower value of E_{a-1C} for the case of the CF₂H-containing substrate significantly facilitates the silylmatalation process, allowing it to afford the corresponding hydrosilylation product smoothly. Thus, it can be concluded that fluorine atoms substituted at the α -position of acetophenone play a pivotal role in decreasing the activation energy required to cross **TS-1** and, thereby, dramatically facilitates the cobalt-catalyzed hydrosilylation reaction.

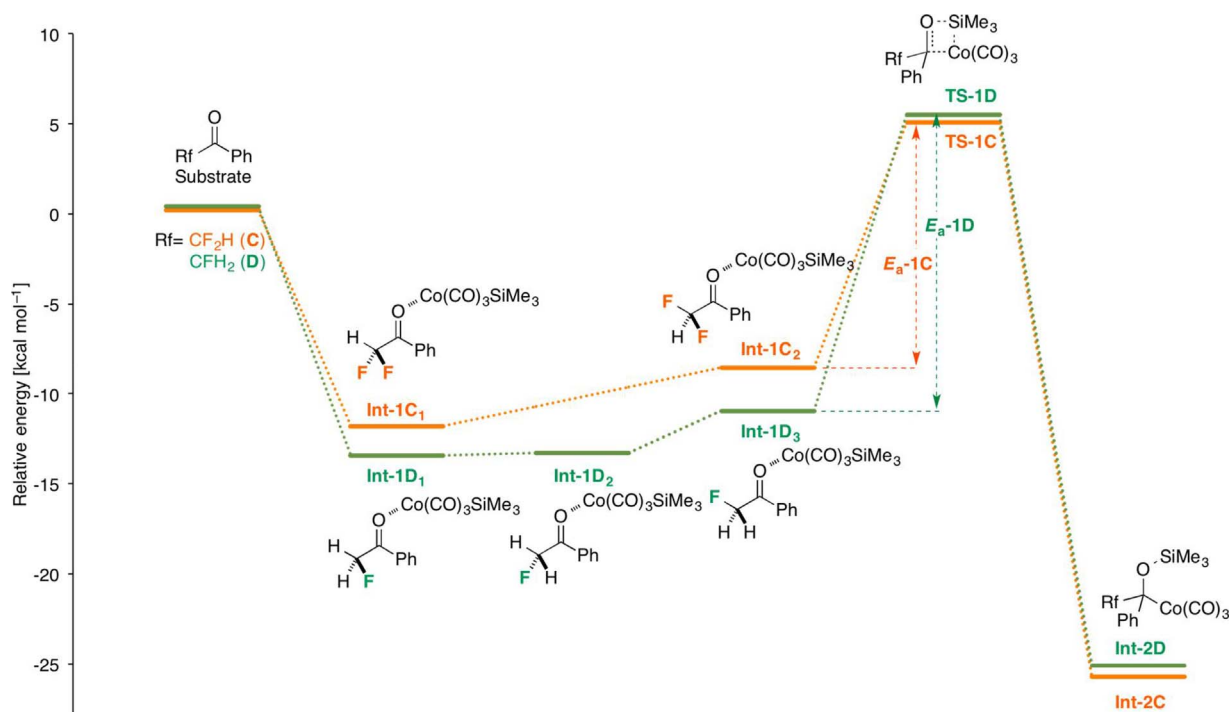


Fig. 4. Energy profile for the hydrosilylation of CF₂H- (**C**) and CFH₂-substituted (**D**) substrates calculated by IRC analysis.

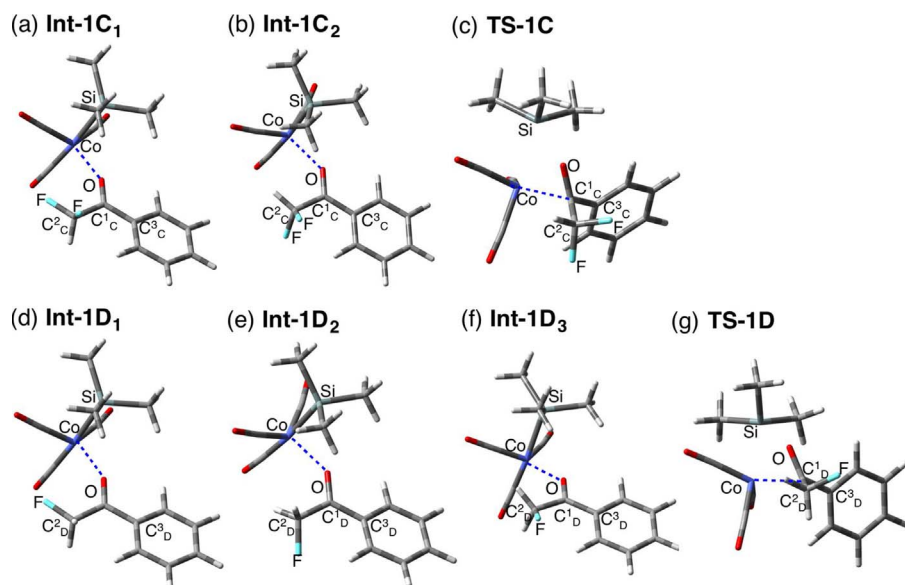


Fig. 5. (a, b) Energy-minimum geometries for Int-1C (with a CF₂H moiety) calculated by IRC analysis, (c) geometries for TS-1C, (d–f) energy-minimum geometries for Int-1D (with a CFH₂ moiety) calculated by IRC analysis, and (g) geometries for TS-1D.

3. Conclusion

In this study, we have demonstrated that replacement of hydrogen atoms at the α -position of acetophenone derivatives by fluorine atoms made it possible to proceed cobalt-catalyzed silylmatalation reactions, and we have elucidated the effects of fluorine substitution by theoretical calculations. Cobalt-catalyzed hydrosilylation of α,α,α -trifluoro- or α,α -difluoroacetophenone derivatives with Et₃SiH occurred smoothly to provide the corresponding hydrosilylated products in high yields, whereas no reaction occurred when non-fluorinated or α -fluoroacetophenone derivatives were used as substrates. In addition, various α,α,α -trifluoroacetophenone derivatives having an electron-donating or -withdrawing substituent on the aromatic ring also participated well in cobalt-catalyzed hydrosilylation, leading to fluorinated silyl ether derivatives in good to excellent yields. From theoretical evaluation using DFT calculations, the dramatic difference between the fluorinated and non-fluorinated substrates was found to significantly influence the activation energy required to cross the transition state in the silylmatalation process; increasing fluorine substitution at the α -position of acetophenone derivatives causes a dramatic decrease in the activation energy. The findings obtained in this study provide valuable information on the fluorine-substitution effect in organofluorine molecules and will facilitate the design and development of new organic materials as well as pharmaceuticals consisting of organofluorine compounds.

4. Experimental

4.1. General experimental procedures

Infrared spectra (IR) were determined in a liquid film on a NaCl plate with a JASCO FT/IR-4100 type A spectrometer and all spectra are reported in wavenumber (cm⁻¹). ¹H and ¹³C NMR spectra were measured with a Bruker AVANCE III 400 NMR spectrometer (¹H: 400 MHz and ¹³C: 100 MHz) in chloroform-*d* (CDCl₃) solution and the chemical shifts are reported in parts per million (ppm) using the residual proton in the NMR solvent. ¹⁹F NMR (376 MHz) spectra were measured with a Bruker AVANCE III 400 NMR spectrometer in CDCl₃ solution with CFCl₃ ($\delta_F = 0$ ppm) as an internal standard. The Bruker AVANCE III 400 NMR spectrometer was used for determining the yield of the products with trifluoromethylbenzene (CF₃C₆H₅) or hexafluorobenzene (C₆F₆). High-resolution mass spectra (HRMS) were taken on a JEOL JMS-700MS spectrometer with fast atom bombardment (FAB) methods.

4.1.1. Materials

All reactions were carried out using dried glassware with a magnetic stirrer bar and routinely monitored by ¹⁹F NMR spectroscopy or thin-layer chromatography (TLC). All chemicals were of reagent grade and, if necessary, were purified in the usual manner prior to use. Column chromatography was carried out on silica gel (Wako gel[®] 60N, 38–100 μ m) and TLC analysis was performed on silica gel TLC plates (Merck, Silica gel 60F₂₅₄).

Table 6
Structural data for Int-1 and TS-1 for 1dA and 1eA calculated by DFT calculation.

	For difluorinated 1dA			For monofluorinated 1eA			
	Int-1C ₁	Int-1C ₂	TS-1C	Int-1D ₁	Int-1D ₂	Int-1D ₃	TS-1D
$\angle C^1-O-Co$ [°]	151.1	139.5	–	147.8	136.6	135.1	–
ϕ (C ² –C ¹ –O–Co) [°]	9.9	9.6	–	8.7	1.1	9.4	–
Co...O [pm]	217	214	–	218	213	212	–
Co...C ¹ [pm]	–	–	204	–	–	–	206
$\angle C^2-C^1-O$ [°]	119.8	116.9	110.1	121.3	116.7	116.8	113.4
$\angle C^2-C^1-C^3$ [°]	118.2	121.3	115.5	117.9	123.4	123.1	115.2
$\angle C^3-C^1-O$ [°]	121.9	121.7	121.3	120.8	119.9	120.0	120.7

4.2. Typical procedure for the cobalt-catalyzed hydrosilylation of fluorinated ketones

In a 30 mL two-necked round bottomed-flask, equipped with a magnetic stirring bar, reflux condense and an inlet tube for argon, were placed 2,2,2-trifluoro-4'-methylacetophenone (**1aA**, 0.092 g, 0.49 mmol) and triethylsilane (0.10 mL, 0.63 mmol) and $\text{Co}_2(\text{CO})_8$ (1.7 mg, 5.0 μmol) in toluene (2.5 mL), and the whole was stirred at reflux temperature. After 3 h, the reaction mixture was subjected to a flash column chromatography using a silica gel as a stationary phase and AcOEt as a mobile phase. After removal of solvent from the eluent using a rotary evaporator under reduced pressure, the residue obtained was purified by silica gel column chromatography (hexane/AcOEt = 50/1) to give the corresponding triethyl[2,2,2-trifluoro-1-(4-methylphenyl)ethoxy]silane **2aA** in 84% yield (0.13 g, 0.41 mmol) as a colorless oil.

4.2.1. Triethyl[2,2,2-trifluoro-1-(4-methylphenyl)ethoxy]silane (**2aA**)

Yield: 84% (colorless oil); IR (neat): ν 2958, 2915, 2880, 1273, 1205, 1170, 1132, 1108, 1007, 842 cm^{-1} ; HRMS (FAB): calcd for $[\text{M}^+]$ $\text{C}_{15}\text{H}_{23}\text{F}_3\text{OSi}$: 304.1470, Found: 304.1466; ^1H NMR: δ 0.53–0.70 (m, 6H), 0.94 (t, $J = 7.9$ Hz, 9H), 2.39 (s, 3H), 4.93 (q, $J = 6.5$ Hz, 1H), 7.20 (d, $J = 7.9$ Hz, 2H), 7.37 (d, $J = 7.9$ Hz, 2H); ^{13}C NMR: δ 4.7, 6.6, 21.4, 73.4 (q, $J = 32.0$ Hz), 124.5 (q, $J = 282.3$ Hz), 127.6, 129.1, 132.9, 139.1; ^{19}F NMR: δ -79.60 (d, $J = 6.5$ Hz, 3F).

4.2.2. Triethyl(2,2,2-trifluoro-1-phenylethoxy)silane (**2aB**)

Yield: 83% (colorless oil); IR (neat): ν 2959, 2915, 2880, 1457, 1272, 1206, 1170, 1133, 1006, 854 cm^{-1} ; HRMS (FAB): calcd for $[\text{M}^+]$ $\text{C}_{14}\text{H}_{21}\text{F}_3\text{OSi}$: 290.1314, Found: 290.1306; ^1H NMR: δ 0.52–0.67 (m, 6H), 0.90 (t, $J = 7.9$ Hz, 9H), 4.93 (q, $J = 6.6$ Hz, 1H), 7.35–7.40 (m, 3H), 7.43–7.49 (m, 2H); ^{13}C NMR: δ 4.6, 6.5, 73.6 (q, $J = 32.0$ Hz), 124.4 (q, $J = 282.4$ Hz), 127.8, 128.4, 129.2, 135.9; ^{19}F NMR: δ -78.97 (d, $J = 6.6$ Hz, 3F).

4.2.3. Triethyl[2,2,2-trifluoro-1-(4-methoxyphenyl)ethoxy]silane (**2aC**)

Yield: 95% (colorless oil); IR (neat): ν 2958, 2914, 2880, 1614, 1516, 1275, 1207, 1170, 1131, 1036, 843 cm^{-1} ; HRMS (FAB): calcd for $[\text{M}^+]$ $\text{C}_{15}\text{H}_{23}\text{F}_3\text{O}_2\text{Si}$: 320.1419, Found: 320.1411; ^1H NMR: δ 0.52–0.66 (m, 6H), 0.91 (t, $J = 7.9$ Hz, 9H), 3.82 (s, 3H), 4.88 (q, $J = 6.6$ Hz, 1H), 6.90 (d, $J = 8.6$ Hz, 2H), 7.38 (d, $J = 8.6$ Hz, 2H); ^{13}C NMR: δ 4.6, 6.6, 55.3, 73.2 (q, $J = 32.1$ Hz), 113.8, 124.5 (q, $J = 282.3$ Hz), 127.9, 129.0, 160.3; ^{19}F NMR: δ -79.25 (d, $J = 6.6$ Hz, 3F).

4.2.4. Triethyl[2,2,2-trifluoro-1-(3-methoxyphenyl)ethoxy]silane (**2aD**)

Yield: 94% (colorless oil); IR (neat): ν 2958, 2915, 2880, 1604, 1493, 1262, 1242, 1172, 1133, 855, cm^{-1} ; HRMS (FAB): calcd for $[\text{M}^+]$ $\text{C}_{15}\text{H}_{23}\text{F}_3\text{O}_2\text{Si}$: 320.1419, Found: 320.1423; ^1H NMR: δ 0.55–0.68 (m, 6H), 0.91 (t, $J = 7.9$ Hz, 9H), 3.82 (s, 3H), 4.90 (q, $J = 6.4$ Hz, 1H), 6.88–6.96 (m, 1H), 7.00–7.12 (m, 2H), 7.28 (t, $J = 8.1$ Hz, 1H); ^{13}C NMR: δ 4.6, 6.6, 55.3, 73.4 (q, $J = 32.0$ Hz), 113.2, 114.8, 120.1, 124.4 (q, $J = 282.5$ Hz), 129.4, 137.4, 159.7; ^{19}F NMR: δ -78.84 (d, $J = 6.4$ Hz, 3F).

4.2.5. Triethyl[2,2,2-trifluoro-1-(2-methoxyphenyl)ethoxy]silane (**2aE**)

Yield: 80% (colorless oil); IR (neat): ν 2958, 2915, 2880, 1494, 1272, 1248, 1173, 1134, 1030, 849 cm^{-1} ; HRMS (FAB): calcd for $[\text{M}^+]$ $\text{C}_{15}\text{H}_{23}\text{F}_3\text{O}_2\text{Si}$: 320.1419, Found: 320.1409; ^1H NMR: δ 0.50–0.65 (m, 6H), 0.88 (t, $J = 7.9$ Hz, 9H), 3.84 (s, 3H), 5.56 (q, $J = 6.5$ Hz, 1H), 6.88 (dd, $J = 8.4, 0.7$ Hz, 1H), 7.00 (td, $J = 7.5, 0.7$ Hz, 1H), 7.32 (ddd, $J = 8.4, 7.5, 1.7$ Hz, 1H), 7.60 (br s, $J = 7.5$ Hz, 1H); ^{13}C NMR: δ 4.6, 6.5, 55.8, 66.0 (q, $J = 32.8$ Hz), 110.6, 120.8, 124.6, 124.8 (q, $J = 282.5$ Hz), 129.0, 130.1, 156.9; ^{19}F NMR: δ -79.08 (d, $J = 6.5$ Hz, 3F).

4.2.6. Triethyl[2,2,2-trifluoro-1-(4-chlorophenyl)ethoxy]silane (**2aG**)

Yield: 89% (colorless oil); IR (neat): ν 2959, 2915, 2880, 1494, 1280, 1242, 1172, 1135, 1092, 860 cm^{-1} ; HRMS (FAB): calcd for $[\text{M} + \text{H}]^+$ $\text{C}_{14}\text{H}_{21}\text{ClF}_3\text{OSi}$: 325.1002, Found: 325.0992; ^1H NMR: δ 0.55–0.65 (m, 6H), 0.91 (t, $J = 7.9$ Hz, 9H), 4.91 (q, $J = 6.4$ Hz, 1H), 7.36 (d, $J = 8.7$ Hz, 2H), 7.40 (d, $J = 8.7$ Hz, 2H); ^{13}C NMR: δ 4.5, 6.4, 72.8 (q, $J = 32.8$ Hz), 124.0 (q, $J = 282.4$ Hz), 128.6, 128.9, 134.2, 135.1; ^{19}F NMR: δ -79.09 (d, $J = 6.4$ Hz, 3F).

4.2.7. Triethyl[2,2,2-trifluoro-1-(1-naphthyl)ethoxy]silane (**2aH**)

Yield: 95% (colorless oil); IR (neat): ν 2958, 2914, 2879, 1272, 1235, 1173, 1131, 1007, 852, cm^{-1} ; HRMS (FAB): calcd for $[\text{M}]^+$ $\text{C}_{18}\text{H}_{23}\text{F}_3\text{OSi}$: 340.1470, Found: 340.1465; ^1H NMR: δ 0.55–0.69 (m, 6H), 0.90 (t, $J = 7.9$ Hz, 9H), 5.82 (q, $J = 5.9$ Hz, 1H), 7.55–7.60 (m, 3H), 7.85–7.93 (m, 3H), 8.13 (d, $J = 8.0$ Hz, 1H); ^{13}C NMR: δ 4.6, 6.6, 69.50–70.80 (m, Ar-CH(OH)CF₂), 123.1, 124.9 (q, $J = 283.3$ Hz), 125.3, 125.8, 126.6, 127.0, 129.1, 129.9, 131.2, 131.7, 133.8; ^{19}F NMR: δ -78.36 (brs, 3F).

4.2.8. Triethyl[2,2,3,3,4,4,4-heptafluoro-1-(4-methylphenyl)butoxy]silane (**2bA**)

Yield: Quant. (colorless oil); IR (neat): ν 2959, 2916, 2881, 1460, 1222, 1195, 1133, 1007, 970 cm^{-1} ; HRMS (FAB): calcd for $[\text{M}]^+$ $\text{C}_{17}\text{H}_{23}\text{F}_7\text{OSi}$: 404.1406, Found: 404.1414; ^1H NMR: δ 0.48–0.57 (m, 6H), 0.87 (t, $J = 7.9$ Hz, 9H), 2.37 (s, 3H), 5.09 (dd, $J = 17.2, 5.2$ Hz, 1H), 7.18 (d, $J = 7.9$ Hz, 2H), 7.32 (d, $J = 7.9$ Hz, 2H); ^{13}C NMR: δ 4.7, 6.5, 21.4, 73.2 (dd, $J = 30.5, 22.1$ Hz), 109.9 (tq, $J = 268.7, 37.5$ Hz), 114.7 (dddd, $J = 263.8, 251.5, 31.8, 25.6$ Hz), 119.6 (tt, $J = 287.8, 33.4$ Hz), 128.5, 129.0, 132.3, 139.3; ^{19}F NMR: δ -126.96 (dm, $J = 289.9$ Hz, 1F), -126.75 (dm, $J = 281.5$ Hz, 1F), -124.03 (dm, $J = 289.8$ Hz, 1F), -118.04 (dm, $J = 281.5$ Hz, 1F), -81.40 (dd, $J = 12.4, 9.1$ Hz, 3F).

4.2.9. Triethyl[2,2-difluoro-1-(4-methylphenyl)ethoxy]silane (**2dA**)

Yield: 97% (colorless oil); IR (neat): ν 2957, 2914, 2879, 1459, 1414, 1241, 1118, 1102, 1007, 842 cm^{-1} ; HRMS (FAB): calcd for $[\text{M} + \text{Na}]^+$ $\text{C}_{15}\text{H}_{24}\text{F}_2\text{NaOSi}$: 309.1462, Found: 309.1452; ^1H NMR: δ 0.52–0.66 (m, 6H), 0.91 (t, $J = 7.9$ Hz, 9H), 2.36 (s, 3H), 4.67–4.74 (m, 1H), 5.61 (ddd, $J = 56.9, 55.8, 5.0$ Hz, 1H), 7.18 (d, $J = 7.9$ Hz, 2H), 7.29 (d, $J = 7.9$ Hz); ^{13}C NMR: δ 4.8, 6.7, 21.3, 74.4 (dd, $J = 26.7, 23.5$ Hz), 116.3 (dd, $J = 248.1, 244.4$ Hz), 127.2, 129.2, 134.7 (d, $J = 5.2$ Hz), 138.4; ^{19}F NMR: δ -127.66 (ddd, $J = 277.9, 56.9, 10.9$ Hz, 1F), -125.59 (ddd, $J = 277.9, 55.8, 8.3$ Hz, 1F).

4.3. Computational details

All calculations were carried out using the Gaussian 09 program (Rev. C.01) and density functional theory (DFT) method. We used the standard basis set, 6-31+G(d,p) levels of theory for the geometry optimizations. All stationary points on the potential energy surfaces were ascertained to be the minima or transition states.

References

- [1] (a) For representative books and reviews on transition-metal-catalyzed hydrosilylation, see: Y. Nakajima, S. Shimada, Hydrosilylation reaction of olefins: recent advances and perspectives, RSC Adv. 5 (2015) 20603–20616; (b) B. Marciniak (Ed.), Hydrosilylation, A Comprehensive Review on Recent Advances, Springer, Netherlands, 2009; (c) S. Díez-González, S.P. Nolan, Transition metal-catalyzed hydrosilylation of carbonyl compounds and imines. A review, Org. Prep. Proc. Int. (2007), pp. 523–559; (d) A.K. Roy, A Review of Recent Progress in Catalyzed Homogeneous Hydrosilylation (Hydrosilylation), Adv. Organomet. Chem. (2008), pp. 1–59.
- [2] (a) A.J. Holwell, For platinum- or palladium-catalyzed hydrosilylation, see: Platin. Met. Rev. 52 (2008) 243–246; (b) M. Igarashi, T. Fuchikami, Transition-metal complex-catalyzed reduction of amides with hydrosilanes: a facile transformation of amides to amines, Tetrahedron Lett. 42 (2001) 1945–1947.

- [3] (a) K. Riener, M.P. Högerl, P. Giegler, F.E. Kühn, Rhodium-catalyzed hydrosilylation of ketones: catalyst development and mechanistic insights, For rhodium-catalyzed hydrosilylation, see: *ACS Catal.* 2 (2012) 613–621;
 (b) M. Sawamura, R. Kuwano, Y. Ito, trans-Chelating chiral diphosphane ligands bearing flexible P-Alkyl substituents (AlkylTRAPs) and their application to the rhodium-catalyzed asymmetric hydrosilylation of simple ketones, *Angew. Chem. Int. Ed.* 33 (1994) 111–113;
 (c) H. Nishiyama, H. Sakaguchi, T. Nakamura, M. Horiyama, M. Kondo, K. Itoh, Chiral and C2-symmetrical bis(oxazolonylpyridine)rhodium(III) complexes: effective catalysts for asymmetric hydrosilylation of ketones, *Organometallics* 8 (1989) 846–848.
- [4] (a) G. Zhu, M. Terry, X. Zhang, Asymmetric hydrosilylation of ketones catalyzed by ruthenium complexes with chiral tridentate ligands, For ruthenium-catalyzed hydrosilylation, see: *J. Organomet. Chem.* 547 (1997) 97–101;
 (b) Y. Nishibayashi, I. Takei, S. Uemura, M. Hidai, Ruthenium-catalyzed asymmetric hydrosilylation of ketones and imine, *Organometallics* 17 (1996) 3420–3422.
- [5] (a) R. Malacea, R. Poli, E. Manoury, Asymmetric hydrosilylation, transfer hydrogenation and hydrogenation of ketones catalyzed by iridium complexes, For iridium-catalyzed hydrosilylation, see: *Coord. Chem. Rev.* 254 (2010) 729–752;
 (b) A.R. Chianese, R.H. Crabtree, Axially chiral bidentate n-heterocyclic carbene ligands derived from BINAM: rhodium and iridium complexes in asymmetric ketone hydrosilylation, *Organometallics* 24 (2005) 4432–4436.
- [6] (a) M.D. Greenhalgh, A.S. Jones, S.P. Thomas, Iron-catalyzed hydrofunctionalisation of alkenes and alkynes, For a selected review of Fe-catalyzed hydrosilylation, see, *ChemCatChem* 7 (2015) 190–222;
 (b) M. Zhang, A. Zhang, Iron-catalyzed hydrosilylation reactions, *Appl. Organomet. Chem.* 24 (2010) 751–757;
 (c) R.H. Morris, Asymmetric hydrogenation, transfer hydrogenation and hydrosilylation of ketones catalyzed by iron complexes, *Chem. Soc. Rev.* 38 (2009) 2282–2291.
- [7] (a) J. Sun, L. Deng, Cobalt complex-catalyzed hydrosilylation of alkenes and alkynes, For a selected review of co-catalyzed hydrosilylation, see: *ACS Catal.* 6 (2016) 290–300;
 (b) X. Du, Z. Huang, Advances in base-metal-catalyzed alkene hydrosilylation, *ACS Catal.* 7 (2017) 1227–1243;
 (c) Q. Niu, H. Sun, X. Li, H.-F. Klein, U. Flörke, Synthesis and catalytic application in hydrosilylation of the complex *mer*-hydrido(2-mercaptobenzoyl)tris(trimethylphosphine)cobalt(III), *Organometallics* 32 (2013) 5235–5238.
- [8] (a) S.-B. Qi, M. Li, S. Li, J.-N. Zhou, J.-W. Wu, F. Yu, X.-C. Zhang, A.S.C. Chan, J. Wu, Copper-dipyridylphosphine-catalyzed hydrosilylation: enantioselective synthesis of aryl- and heteroaryl cycloalkyl alcohols, For selected examples of copper-catalyzed hydrosilylation, see: *Org. Biomol. Chem.* 11 (2013) 929–937;
 (b) Y.-Z. Sui, X.-C. Zhang, J.-W. Wu, S. Li, J.-N. Zhou, M. Li, W. Fang, A.S.C. Chan, J. Wu, Cu^{II}-Catalyzed asymmetric hydrosilylation of diaryl- and aryl heteroaryl ketones: application in the enantioselective synthesis of orphenadrine and neobonidine, *Chem. Eur. J.* 18 (2012) 7486–7492;
 (c) K. Junge, B. Wendt, D. Addis, S. Zhou, S. Das, M. Beller, Copper-catalyzed enantioselective hydrosilylation of ketones by using monodentate binaphthophosphine ligands, *Chem. Eur. J.* 16 (2010) 68–73;
 (d) X.-C. Zhang, Y. Wu, F.-F. Yu, F. Wu, J. Wu, A.S.C. Chan, Application of copper(II)-dipyridylphosphine catalyst in the asymmetric hydrosilylation of simple ketones in air, *Chem. Eur. J.* 15 (2009) 5888–5891;
 (e) S. Diez-Gonzalez, S.P. Nolan, Copper, silver, and gold complexes in hydrosilylation reactions, *Acc. Chem. Res.* 41 (2008) 349–358;
 (f) B.H. Lipshutz, B.A. Frieman, A.E. Tomaso Jr., Copper-in-charcoal (Cu/C): heterogeneous, copper-catalyzed asymmetric hydrosilylations, *Angew. Chem. Int. Ed.* 45 (2006) 1259–1264.
- [9] (a) S. Yamada, M. Morita, T. Konno, Multi-color photoluminescence induced by electron-density distribution of fluorinated bistolane derivatives, *J. Fluor. Chem.* 202 (2017) 54–64;
 (b) S. Yamada, S. Yamaguchi, O. Tsutsumi, Electron-density distribution tuning for enhanced thermal stability of luminescent gold complexes, *J. Mater. Chem. C* 5 (2017) 7977–7984;
 (c) S. Yamada, K. Miyano, T. Konno, T. Agou, T. Kubota, T. Hosokai, Fluorine-containing bistolanes as light-emitting liquid crystalline molecules, *Org. Biomol. Chem.* 15 (2017) 5949–5958;
 (d) S. Yamada, S. Hashishita, H. Konishi, Y. Nishi, T. Kubota, T. Asai, T. Ishihara, T. Konno, Unprecedented 3,6-disubstituted 1,1,2,2-tetrafluorocyclohexane derivatives, *J. Fluor. Chem.* 200 (2017) 47–58;
 (e) S. Yamada, K. Kinoshita, S. Iwama, T. Yamazaki, T. Kubota, T. Yajima, K. Yamamoto, S. Tahara, Synthesis of perfluoroalkylated pentacenes and evaluation of their fundamental physical properties, *Org. Biomol. Chem.* 15 (2017) 2522–2535;
 (f) S. Yamada, S. Hashishita, T. Asai, T. Ishihara, T. Konno, Design, synthesis, and evaluation of new fluorinated liquid crystals bearing CF₂CF₂ fragment with negative electronic anisotropy, *Org. Biomol. Chem.* 15 (2017) 1495–1509.
- [10] (a) Y. Sakaguchi, S. Yamada, T. Konno, T. Agou, T. Kubota, Stereochemically defined various multi-substituted alkenes bearing a tetrafluoroethylene (–CF₂CF₂–) fragment, *J. Org. Chem.* 82 (2017) 1618–1631;
 (b) K. Tamamoto, S. Yamada, M. Higashi, T. Konno, T. Ishihara, Radical reactivity of α,β -trifluorocyclopropyl ester: facile approach to γ -silyloxy- α,β,β -trifluorobutyric acid derivatives involving regioselective nucleophilic radical addition reaction, *J. Fluorine Chem.* 190 (2016) 23–30;
 (c) S. Yamada, M. Higashi, T. Konno, T. Ishihara, Straightforward and highly stereoselective synthesis of 3,3,4-trifluoropyrrolidines involving 1, 3-dipolar cycloaddition with 2,2, 3-trifluoroacrylate, *Eur. J. Org. Chem.* (2016) 4561–4568;
 (d) S. Yamada, K. Hondo, T. Konno, T. Ishihara, Concise preparation of fluorine-containing carbocycles involving Diels-Alder reaction using fluorinated alkene or diene derivatives, *RSC Adv.* 6 (2016) 28458–28469;
 (e) T. Nihei, Y. Nishi, N. Ikeda, S. Yokotani, T. Ishihara, S. Arimitsu, T. Konno, Highly stereoselective synthesis of fluoroalkene dipeptides via the novel Cr(II)-mediated carbon-fluorine bond cleavage/new carbon–carbon bond formation, *Synthesis* 48 (2016) 865–881 and references cited therein.
- [11] (a) T. Konno, Trifluoromethylated internal alkynes: versatile building blocks for the preparation of various fluorine-containing molecules, *Synlett* (2014) 1350–1370;
 (b) T. Nihei, Y. Kubo, T. Ishihara, T. Konno, Highly regioselective S_N2' reaction of β -fluoroallylic phosphates with organocopper reagents, and its application to the synthesis of fluorine-containing carbocycles, *J. Fluor. Chem.* 167 (2014) 110–121;
 (c) T. Konno, M. Kishi, T. Ishihara, S. Yamada, Stereoselective synthesis of CF₃-substituted trans- and cis-enediynes via carbocupration or hydrostannation reactions of CF₃-containing diyne, *Tetrahedron* 70 (2014) 2455–2463;
 (d) T. Konno, R. Kinugawa, T. Ishihara, S. Yamada, A remarkable regiocontrol in the palladium-catalyzed silylstannylation of fluoroalkylated alkynes – highly regio- and stereoselective synthesis of multi-substituted fluorine-containing alkenes, *Org. Biomol. Chem.* 12 (2014) 1611–1617;
 (e) A. Morigaki, M. Kawamura, S. Arimitsu, T. Ishihara, T. Konno, Application to tertiary amines synthesized by catalytic dehydrogenation of enamines as nucleophilic C₂ synthons for 1,4-conjugate addition with fluoroalkylated olefins, *Asian J. Org. Chem.* 2 (2013) 239–243;
 (f) A. Morigaki, K. Tsukade, S. Arimitsu, T. Konno, T. Kubota, Unusual annulation reaction of electron-deficient alkenes with enamines: an easy access to stereocontrolled 4-fluoroalkylated 3,4-dihydro-2H-pyrans, *Tetrahedron* 69 (2013) 1521–1525;
 (g) A. Morigaki, T. Tanaka, T. Miyabe, T. Ishihara, T. Konno, Rhodium(I)-catalyzed 1,4-conjugate addition toward β -fluoroalkylated electron-deficient alkenes: a new entry to a construction of a tertiary carbon center possessing a fluoroalkyl group, *Org. Biomol. Chem.* 11 (2013) 586–595;
 (h) T. Konno, T. Kida, A. Tani, T. Ishihara, A novel synthesis of fluorine-containing cyclopropanones via Pauson-Khand reaction, *J. Fluor. Chem.* 144 (2012) 147–156;
 (i) T. Konno, K. Moriyasu, R. Kinugawa, T. Ishihara, Rhodium-catalyzed [2 + 2 + 2] cycloaddition of various fluorine-containing alkynes – novel synthesis of multi-substituted fluoroalkylated aromatic compounds, *Org. Biomol. Chem.* 8 (2010) 1718–1724 and references cited therein.
- [12] (a) T. Konno, K. Taku, S. Yamada, K. Moriyasu, T. Ishihara, *Org. Biomol. Chem.* 7 (2009) 1167–1170;
 (b) N. Ikeda, T. Konno, Highly regio- and stereoselective hydrosilylation of β -fluoroalkylated α,β -unsaturated ketones, *J. Fluor. Chem.* 173 (2015) 69–76.
- [13] (a) Recent reports on hydrosilylation of α,α,α -trifluoroacetophenone using tris(pentafluorophenyl)borane as a catalyst, see: N.D. Rio, M. Lopez-Reyes, A. Baceiredo, N. Saffon-Merceron, D. Lutters, T. Müller, T. Kato, *Angew. Chem. Int. Ed.* 56 (2017) 1365–1370;
 (b) I. Mallov, D.W. Stephan, *Dalton Trans.* 45 (2016) 5568–5574.
- [14] (a) F.E. Herkes, D.J. Burton, Fluoro olefins. I. Synthesis of β -substituted perfluoro olefins, *J. Org. Chem.* 32 (1967) 1311–1318;
 (b) A. Kalusznyer, Cyclic analogs of DDT-like compounds, *J. Org. Chem.* 25 (1960) 473–474.
- [15] (a) The electron-withdrawing nature of a substituent can be quantitatively evaluated using the Hammett substituent constant (σ), and the σ_p values for CO₂Et and CF₃ are reported as +0.46 and +0.54, demonstrating the similar electron-withdrawing characteristics of these substituent, see: C. Hansch, A. Leo, R.W. Taft, A survey of Hammett substituent constants and resonance and field parameters, *Chem. Rev.* 91 (1991) 165–195;
 (b) L.P. Hammett, The effect of structure upon the reactions of organic compounds. Benzene derivatives, *J. Am. Chem. Soc.* 59 (1937) 96–103.
- [16] A.J. Chalk, J.F. Harrod, Homogeneous catalysis. IV. Some reactions of silicon hydrides in the presence of cobalt carbonyls, *J. Am. Chem. Soc.* 89 (1967) 1640–1647.
- [17] (a) For related reports on the mechanisms of transition-metal-catalyzed hydrosilylation, see: For Mn catalyst: T.K. Mukhopadhyay, C.L. Rock, M. Hong, D.C. Ashley, T.L. Groy, M.-H. Baik, R.J. Trovitch, Mechanistic investigation of bis(imino)pyridine manganese catalyzed carbonyl and carboxylate hydrosilylation, *J. Am. Chem. Soc.* 139 (2017) 4901–4915;
 (b) For Ru catalyst: M.C. Lipke, T.D. Tilley, Hypercoordinate ketone adducts of electrophilic η^3 -H₂SiRR' Ligands on ruthenium as key intermediates for efficient and robust catalytic hydrosilylation, *J. Am. Chem. Soc.* 136 (2014) 16387–16398;
 (c) D.V. Gutsulyak, S.F. Vyboshchikov, G.I. Nikonov, Cationic silane σ -complexes of ruthenium with relevance to catalysis, *J. Am. Chem. Soc.* 132 (2010) 5950–5951;
 (d) For Rh catalyst: I. Ojima, M. Nihonyanagi, T. Kogure, M. Kumagai, S. Horiuchi, K. Nakatsugawa, Y. Nagai, Reduction of carbonyl compounds via hydrosilylation: I. Hydrosilylation of carbonyl compounds catalyzed by tris(triphenylphosphine)chlororhodium, *J. Organomet. Chem.* 94 (1975) 449–461;
 (e) J.A. Osborn, F.H. Jardine, J.F. Young, G. Wilkinson, The preparation and properties of tris(triphenylphosphine)halogenorhodium(I) and some reactions thereof including catalytic homogenous hydrogenation of olefins and acetylenes and their derivatives, *J. Chem. Soc. A* (1966) 1711–1732.
- [18] M.J. Frish, G.W. Trucks, H.B. Schlegel, G.E. Scuseria, M.A. Robb, J.R. Cheeseman, G. Scalmani, V. Barone, B. Mennucci, G.A. Peterson, H. Nakatsuji, M. Caricato, X. Li, H.P. Hratchian, A.F. Izmaylov, J. Bloino, G. Zheng, J.L. Sonnenberg, M. Hada, M. Ehara, K. Toyota, R. Fukuda, J. Hasegawa, M. Ishida, T. Nakajima, Y. Honda, O. Kitao, H. Nakai, T. Vreven, J.A. Montgomery Jr., J.E. Peralta, F. Ogliaro, M. Bearpark, J.J. Heyd, E. Brothers, K.N. Kudin, V.N. Staroverov, T. Keith,

- R. Kobayashi, J. Normand, K. Raghavachari, A. Rendell, J.C. Burant, S.S. Iyengar, J. Tomasi, M. Cossi, N. Rega, J.M. Millam, M. Klene, J.E. Knox, J.B. Cross, V. Bakken, C. Adamo, J. Jaramillo, R. Gomperts, R.E. Stratmann, O. Yazyev, A.J. Austin, R. Cammi, C. Pomelli, J.W. Ochterski, R.L. Martin, K. Morokuma, V.G. Zakrzewski, G.A. Voth, P. Salvador, J.J. Dannenberg, S. Dapprich, A.D. Daniels, O. Farkas, J.B. Foresman, J.V. Ortiz, J. Gioslowski, D.J. Fox, Gaussian 09W, Revision C.01, Gaussian, Inc., Wallingford CT, 2013.
- [19] (a) H.P. Hratchian, H.B. Schlegel, Accurate reaction paths using a Hessian based predictor-corrector integrator, *J. Chem. Phys.* 120 (2004) 9918–9924;
(b) C. Gonzalez, H.B. Schlegel, An improved algorithm for reaction path following, *J. Chem. Phys.* 90 (1989) 2154–2161;
- (c) K. Fukui, The path of chemical reactions – the IRC approach, *Acc. Chem. Res.* 14 (1981) 363–368.
- [20] J.A. MacPhee, A. Panaye, J.-E. Dubois, Steric effects – I: A critical examination of the taft steric parameter – Es. Definition of a revised, broader and homogeneous scale. Extension to highly congested alkyl groups, *Tetrahedron* 34 (1978) 3553–3562. The steric bulkiness of the substituents around the carbonyl moiety are in the order Ph ($E_s' = -2.31$) > CF_3 ($E_s' = -0.78$) > CH_3 ($E_s' = 0$) A larger negative E_s' value indicates a larger steric effect, see:.
- [21] The calculation results of Int-2C and Int-2D were described in the supporting information.